

# Chain terminal group leads to distinct thermoresponsive behaviors of linear PNIPAM and polymer analogs

Xiaolong Lang<sup>a</sup>, Alexander D. Patrick<sup>a</sup>, Boualem Hammouda<sup>b</sup>, Michael J.A. Hore<sup>a,\*</sup>

<sup>a</sup> Department of Macromolecular Science and Engineering, Case Western Reserve University, 10900 Euclid Avenue, Cleveland, OH, 44106, USA

<sup>b</sup> NIST Center for Neutron Research, 100 Bureau Drive, Gaithersburg, MD, 20899, USA

## ARTICLE INFO

### Article history:

Received 23 February 2018

Received in revised form

13 April 2018

Accepted 26 April 2018

Available online 28 April 2018

### Keywords:

PNIPAM

Thermoresponsive

Neutron scattering

## ABSTRACT

Poly(alkylacrylamides), most notably poly(*N*-isopropylacrylamide) (PNIPAM), are widely studied thermoresponsive polymers. Linear PNIPAM, poly(*N*-*n*-propylacrylamide) (PNnPAM) and poly(*N*-cyclopropylacrylamide) (PNCPAM) were synthesized via RAFT polymerization to obtain polymers with low dispersity and varying terminal groups. The polymers were studied with a combination of small-angle neutron scattering (SANS), turbidimetry measurements, and dissipative particle dynamics (DPD) simulations to determine the influence of terminal group and monomer structure on assembly and thermoresponsive behavior in solution. Large scale, fractal assemblies (larger than 1 μm) are observed below the critical temperature for polymers terminated with short hydrophobic groups, but for long hydrophobic terminal groups, polymers formed small micelles (*ca.* 15 nm). The two cases give rise to two distinct thermoresponsive behaviors: the fractal assemblies display the traditional coil-to-globule behavior, whereas the corona of the micelles collapsed well below the critical temperature due to *n*-clustering, while the micelles remained in solution. The results indicate that, despite making up only a small fraction of the polymer, the terminal groups play a large role in both the conformation and assembly of PNIPAM and its analogs below the critical temperature, and hints at the possibility of new design strategies for thermoresponsive materials.

© 2018 Elsevier Ltd. All rights reserved.

## 1. Introduction

Thermoresponsive polymers have attracted a large amount of attention in the polymer community due to their potential applications, most notably in the biomedical field [1–3]. Aqueous solutions of poly(*N*-alkylacrylamide)s undergo a reversible coil-to-globule transition when heated above their lower critical solution temperature (LCST). Poly(*N*-isopropylacrylamide) (PNIPAM), in particular, has been most widely studied because of its LCST of  $T_C \approx 32^\circ\text{C}$ , which is close to physiological conditions [4]. Many studies have been carried out to understand the coil-to-globule transformation of PNIPAM in water, and the PNIPAM/water phase diagram [5–10]. The thermoresponsiveness of PNIPAM comes from its amphiphilic structure. The hydrophilic secondary amine group of PNIPAM can form hydrogen bonds with water molecules, and hydrophobic isopropyl group is hydrated below the LCST. The phase transition of PNIPAM is controlled by the balance between

polymer-polymer and polymer-solvent interactions. In addition, the terminal group and molecular weight can influence the LCST of PNIPAM [11–14].

Key to the attractiveness of PNIPAM, and other similar thermoresponsive polymers, are the particular characteristics of the thermoresponsive behavior including the critical temperature, kinetics of the transition, and presence of thermal hysteresis. A comprehensive review by Halperin, Kröger, and Winnik summarizes over fifty years of research into the phase behavior of PNIPAM in water – detailing how factors such as synthesis technique; mass fraction/concentration; molecular weight and dispersity; and measurement technique can lead to differences in reported values of the critical temperature [15]. As one example, turbidimetry measurements of the cloud point of a PNIPAM solution will give a critical temperature near the binodal temperature, whereas determining the critical temperature by extrapolation from small-angle neutron scattering measurements will give the spinodal temperature. Calorimetry measurements find evidence of multiple critical temperatures, depending on the particular system being examined. Notably, recent work from several research groups has

\* Corresponding author.

E-mail address: [hore@case.edu](mailto:hore@case.edu) (M.J.A. Hore).

found that PNIPAM exhibits thermoresponsive behavior well below the LCST near 32 °C. Warr et al. and Štěpánek et al., studied thermo- and pH-responsive dodecyl-terminated PNIPAM that formed micelles in aqueous solutions [16,17]. Winnik et al. examined SANS of hydrophobically modified telechelic PNIPAM at different concentrations. They suggested that octadecyl-terminated PNIPAM formed a three-layered core-shell morphology [18]. Molecular analogs of PNIPAM, such as poly(N-cyclopropylacrylamide) (PNCpAM) and poly(N-n-propylacrylamide) (PNnPAM) have also drawn interest from the scientific community [19,20]. Subtle differences in the substitute group results in large differences in the LCST and phase transition behaviors. Inomata et al. investigated the phase transition of N-substituted acrylamide gels including PNnPAM, PNIPAM and PNCpAM. They found that PNnPAM gels exhibit a lower transition temperature, and much sharper, discontinuous volume transition in comparison to PNIPAM gels, while PNCpAM gels showed a continuous volume transition [20]. The research group lead by Ito and Kubota studied the thermal behavior of PNnPAM in water and observed a drastic decrease of the second virial coefficient near the theta temperature [19,21]. They ascribed this behavior to the increase of chain stiffness of the polymer due to the linear n-propyl group.

Controlled radical polymerization methods such as reversible addition-fragmentation chain transfer (RAFT) polymerization have led to the ability to prepare well-defined, end-functionalized polymer chains that enable many additional studies of poly(-alkylacrylamide) thermoresponsive behavior [22]. We recently studied the interaction and conformation of star-branched PNIPAM, with identical core structures but different terminal groups, by SANS [23], and showed that the conformation of PNIPAM, characterized by an excluded volume parameter  $\nu$ , is largely unaffected by the number of arms of the star and the terminal group for bromine, phenyl, and thiol-terminated polymers. The radius of gyration scales with  $\nu$  as  $R_g \sim N^\nu$ , where  $N$  is the degree of polymerization. In contrast, by fitting the SANS data with a new form factor that explicitly accounts for excluded volume, we found that dodecyl-terminated star PNIPAM collapses to form compact globules below the LCST with  $\nu \approx 0.38$ , while also remaining dispersed in the solution. This observation was particularly intriguing since the terminal group makes up only a small portion of the polymer. Thus, a natural question that arises is that of how the terminal group of linear chains affects the conformation and assembly of PNIPAM in water – the answer to which may have implications for synthesizing thermoresponsive materials from linear chains.

Self-assembled, thermoresponsive soft materials created from linear PNIPAM chains have been studied extensively in the past two decades [24–26]. These associative polymers have been widely studied due to potential applications as a drug carrier [27,28]. Numerous studies have focused on self-assembly in aqueous solutions of PNIPAM and its copolymers, on PNIPAM-grafted nanoparticles, and on mechanisms of tuning both the LCST and micelle structure [29–34]. In the case of PNIPAM-grafted nanoparticles, Shan et al. reported two separate phase transitions of PNIPAM chains that were bound to gold nanoparticles. They ascribed this behavior to the density difference of PNIPAM chains close to and far away from the gold core surface [29]. Chung et al. studied the core-shell micellar structures of alkyl-terminated PNIPAM with different chain lengths (C<sub>3</sub>–C<sub>18</sub>), and found that a hydrophobic alkyl terminal group leads to aggregation of PNIPAM chains at temperatures lower than the LCST of PNIPAM [30]. Zhu's group has successfully synthesized dodecyl-terminated random block copolymers of N-propylacrylamide and N-ethylacrylamide that exhibit double thermoresponsiveness, with LCSTs ranging from 20 to 85 °C, by adjusting the composition of the two segments. Triblock terpolymers of poly(N-n-propylacrylamide)-block-poly(N-

isopropylacrylamide)-block-poly (N, N-ethylmethacrylamide) exhibited a multistep phase transition [31,32]. PNIPAM and PNIPAM containing copolymers can self-assemble into different micelle structures depending on the terminal group, volume fraction and hydrophobicity of the comonomer. When co-blocking PNIPAM with hydrophilic polymers, such as poly(ethylene oxide) (PEO), the resulting copolymer forms micelles with a PNIPAM core [35,36]. In contrast, copolymers incorporating PNIPAM and a hydrophobic block, such as polystyrene (PS) or poly(n-butyl methacrylate) (PBMA), will form micelles with a PNIPAM corona [37–39]. Winnik et al. reported flowerlike micelle with loops of PNIPAM corona synthesized from PNIPAM with long alkyl chains at each end [40]. Similarly, Zhang et al. observed flowerlike micelles with a looped PNIPAM corona when polystyrene-b-poly(N-isopropylacrylamide)-b-polystyrene (PS-b-PNIPAM-b-PS) was dissolved in water, demonstrating the range of structures that can self-assemble from linear PNIPAM-based polymers [41].

In this work, we demonstrate two *distinct* thermal behaviors of three closely related poly(N-alkylacrylamide)s that depend on the terminal group of the polymer, and show that these behaviors occur well below the critical temperatures of the respective polymers. We report the preparation of a series of thermoresponsive poly(N-alkylacrylamide)s including PNIPAM, PNnPAM and PNCpAM by RAFT polymerization, with either a dodecyl or ethyl terminal group, and the characterization of the chain assembly and thermodynamics in aqueous solutions, finding that the dodecyl terminal group leads to the formation of micelles whereas the ethyl group does not. In addition, a series of varying molecular weight dodecyl-terminated PNIPAM is synthesized and characterized with SANS to investigate the relationship between molecular weight and micellization. Unlike light scattering, SANS measurements allow us to perform detailed analysis of the micellar structure of dodecyl-terminated poly(N-alkylacrylamide)s, including the size of the core as well as the size and conformation of the corona, and our analysis yields new insights into these systems that have not been seen previously. We analyze SANS measurements of linear dodecyl-terminated poly(N-alkylacrylamide)s in D<sub>2</sub>O with a spherical core-chain model and demonstrate that the dodecyl group is the driving force for micellization. Ethyl poly(N-alkylacrylamide)s do not form micelles, and are fit according to a form factor for linear polymers with excluded volume, combined with the random phase approximation (RPA) [23]. Our results show that the coronas of dodecyl-terminated poly(N-alkylacrylamide) micelles collapse well below the critical temperature by an *n*-clustering process, despite remaining dispersed in solution. *N*-clustering behavior is defined by a concentration-dependent Flory-Huggins parameter which leads to aggregation of the polymer chains as the monomer concentration increases [42–44]. In contrast, ethyl-terminated chains form large-scale fractal aggregates in solution, but otherwise display only weak thermoresponsive behavior below their critical temperatures as they approach the coil-to-globule transition.

## 2. Experimental and computational methods

**Materials.** Except 2-(Dodecylthiocarbonothioylthio)-2-methylpropionic acid (DDMAT), which was purchased from STREM, all materials were purchased from Sigma Aldrich of the highest quality and used as received unless stated otherwise. N-Isopropylacrylamide (NIPAM) (Aldrich, 97%) was recrystallized from toluene/hexane 3:2 and dried by vacuum before use. PNIPAM, PNCpAM, PNnPAM were prepared by RAFT.

**Synthesis of 2-Ethylsulfanyliothiocarbonylsulfanyl-2-methylpropionic Acid (EDMAT).** Ethanethiol (1.55 g, 25 mmol), acetone (12.65 g, 20.75 mmol), and trioctylmethylammonium chloride (Aliquat 336; 0.404 g, 1 mmol) were mixed in a 250 mL 3

neck round-bottom flask. The flask was placed in an ice/water bath cooled to 5 °C and purged with nitrogen. Sodium hydroxide solution (50%) (2.1 g, 26.25 mmol) was then added over 20 min through a syringe pump. The reaction was stirred for an additional 20 min before carbon disulfide (1.9 g, 25 mmol) in acetone (2.54 g, 43.75 mmol) was added over a 20 min period and the solution turned yellow. After 20 min, chloroform (4.48 g, 37.5 mmol) was added in one portion, followed by dropwise addition of 50% sodium hydroxide solution (10.0 g, 125 mmol) over 30 min. The solution turns orange gradually. The reaction was then allowed to react overnight under room temperature after which time the acetone was removed via rotary evaporation under room temperature to afford an orange-brownish oil. The residue was washed with water three times and then purified through column chromatography (silica gel 60 Å, 70–230 mesh) using ethyl acetate:hexane (2:3 v/v) as an eluent. The solvent was removed under vacuum. The target compound was recrystallized from hexane under –20 °C, resulting in large bright yellow crystals. <sup>1</sup>H NMR (600 MHz, CDCl<sub>3</sub> d): 3.30 (q, 2H), 1.71 (s, 6H), 1.32 (t, 3H). (Fig. S1).

**Synthesis of N-propylacrylamide (NnPAM).** A solution of propylamine (4.73 g, 80 mmol) and triethylamine (8.07 g, 80 mmol) in 50 mL of chloroform was cooled to 0 °C in a nitrogen atmosphere, and acryloyl chloride (7.24 g, 80 mmol) was added dropwise as the temperature was maintained below 5 °C. The reaction was allowed to warm to room temperature overnight. The solution was then washed two times with 10% concentrated HCl solution, three times with brine, and dried with Na<sub>2</sub>SO<sub>4</sub>. The solvent was removed under reduced pressure and the raw product was recrystallized from diethyl ether under –20 °C to yield a white crystal. <sup>1</sup>H NMR (600 MHz, CDCl<sub>3</sub>) δ (ppm) 6.20 (dd, 1H), 6.06 (dd, 1H), 5.53 (dd, 1H), 3.22 (q, 2H), 1.50 (m, 2H), 0.87 (t, 3H). (Fig. S2).

**Synthesis of N-cyclopropylacrylamide (NCPAM).** A solution of cyclopropylamine (4.56 g, 80 mmol) and triethylamine (8.07 g, 80 mmol) in 50 mL of chloroform was cooled to 0 °C in a nitrogen atmosphere, and acryloyl chloride (7.24 g, 80 mmol) was added dropwise as the temperature was maintained below 5 °C. The reaction was allowed to warm to room temperature overnight. The solution was then washed two times with 10% concentrated HCl solution, three times with brine, and dried with Na<sub>2</sub>SO<sub>4</sub>. The solvent was removed under reduced pressure and the raw product was recrystallized from diethyl ether under –20 °C to yield a white crystal. <sup>1</sup>H NMR (600 MHz, CDCl<sub>3</sub>) δ (ppm) 6.23 (d, 1H, CH<sub>2</sub>.dblunds.CH), 6.01 (dd, 5.7 Hz, CHH.dblunds.CH), 5.60 (d, 1H, CHH.dblunds.CH), 2.77 (m, 1H, NHCH), 0.78 (m, 2H, CH<sub>2</sub>), 0.52 (m, 2H, CH<sub>2</sub>). (Fig. S3).

**Polymerization of NnPAM, NIPAM, NCPAM through RAFT.** NIPAM, NCPAM, NnPAM were polymerized by RAFT polymerization. DDMAT and EDMAT were used as chain transfer agents (CTA). Generally, a 4 M solution of N-acrylamide in *N,N*-dimethylformamide (DMF) was prepared with a ratio of CTA to initiator of [CTA]<sub>0</sub>: [AIBN]<sub>0</sub> = 7.5:1. For example, to prepare a EDMAT-PNnPAM with a molecular weight of 20,000 g/mol at 90% conversion, a stock solution of NIPAM (4 M), azobis (isobutyronitrile) (AIBN) (2.73 × 10<sup>-3</sup> M), and chain transfer agent EDMAT (2.05 × 10<sup>-2</sup> M) in DMF was prepared. [NIPAM]<sub>0</sub>: [CTA]<sub>0</sub>: [AIBN]<sub>0</sub> = 195:1:0.13. Generally, 3 mL of stock solution was transferred to 10 mL Schlenk flasks, connected to a nitrogen manifold, and degassed for 30 min in ice water bath. Polymerization was conducted at 70 °C in a constant temperature oil bath for 3 h. The flask was opened to the atmosphere and quenched with ice water to terminate the reaction. For purification, PNnPAM and PNIPAM were dissolved in THF, precipitated with an excess amount of ethyl ether, and then centrifuged for 20 min at 8000 rpm. This precipitation was repeated three times, solvent removed, and the product dried by vacuum to provide polymers with acceptable purity determined by <sup>1</sup>H NMR. The <sup>1</sup>H

NMR of ethyl PNIPAM and PNnPAM are contained in the Supporting Information (Figs. S4 and S5). PNCPAM was dissolved in methanol instead of THF and precipitated in excess amount of ethyl ether for purification. The chemical structures of the polymers are summarized in Fig. 1, and molecular weight control over the PNIPAM series is demonstrated in the SEC-MALS chromatographs in Fig. 2.

**Turbidimetry measurement:** For each polymer, a 0.5 wt% solution in HPLC water was prepared and refrigerated until the polymer was fully dissolved in the solution. A Pike Technologies Peltier-Controlled cuvette holder was used to closely control the temperature, and a 632.8 nm laser diode was used to measure the transmission. Custom in-house software was used to measure the laser intensity as a function of time and temperature using an Arduino microcontroller. The temperature was heated and cooled at the ramp rate of 0.1 °C/min. The cloud point temperature was reported at 90% transmission.

**Size and Molecular Weight Characterization.** The molecular weight and dispersities of the synthesized polymers were determined by SEC-MALS using both a refractive index detector (Wyatt Optilab T-rEX) and an 18-angle light scattering detector (Wyatt Dawn Heleos II) in DMF containing 0.05 mol/L LiBr at a flow rate of 1.0 mL/min. The optical wavelength used by the refractive index and light scattering detectors was 658 nm. The differential index of refraction was measured with T-rEX in DMF with 0.05 mol/L LiBr and determined to be dn/dc = 0.0655 ± 0.0006 mL/g, 0.0712 ± 0.0008 mL/g, 0.0932 ± 0.0007 mL/g for PNIPAM, PNnPAM, PNCPAM at 25 °C, respectively. Terminal group has no effect on the dn/dc value for the same polymer. The dn/dc measurements of dodecyl polymers are included in the Supporting Information (Figs. S6–S8).

**Small-Angle Neutron Scattering (SANS).** SANS was performed on the NGB 30 m SANS instrument at the National Institute of Standards and Technology (NIST) Center for Neutron Research (NCNR, Gaithersburg, MD). Ethyl PNnPAM and PNCPAM were prepared with 1 wt% in both D<sub>2</sub>O (11 mg/mL) and ethanol-d<sub>6</sub> (8.92 mg/mL). High *M<sub>n</sub>* dodecyl PNIPAM samples were prepared with 0.5 wt% in D<sub>2</sub>O (5.5 mg/mL). Scattered neutron intensities were measured as a function of scattering variable *q* at three sample-to-detector distances of 1 m, 4 m, and 13 m. The neutron wavelength was λ = 6 Å. Two-dimensional scattering patterns were radially averaged and corrected for background and empty sample cell scattering using standard methods. The 1D scattering intensities were fit as a function of *q* using one or two different form factors, detailed below, where the scattering variable  $q = (4\pi/\lambda)\sin(\theta/2)$ .

**Polymer With Excluded Volume Model:** Scattering intensities of ethyl terminated PNnPAM, PNCPAM, and PNIPAM were fit using a form factor for a linear polymer with excluded volume. The form

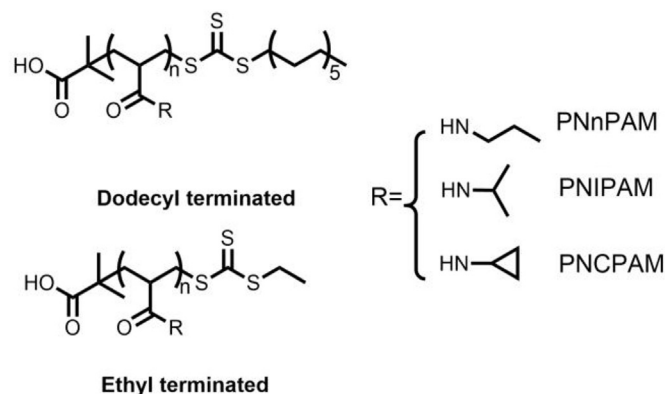


Fig. 1. Structures of ethyl- and dodecyl-terminated PNIPAM, PNnPAM, and PNCPAM.

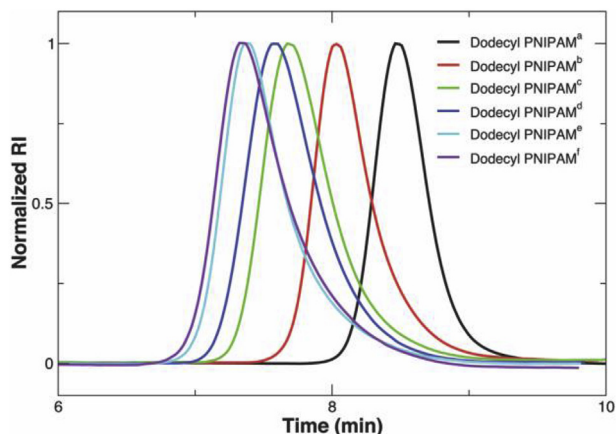


Fig. 2. SEC-MALS chromatogram of dodecyl-PNIPAM (a–f).

factor for linear polymer with excluded volume is given by

$$P(q, N) = 2 \int_0^1 (1-x) \exp \left[ -\frac{q^2 b^2}{6} N^{2\nu} x^{2\nu} \right] dx \quad (1)$$

where  $\nu$  is the excluded volume parameter,  $b$  is the Kuhn length,  $N$  is the degree of polymerization and  $q$  is the scattering variable [45]. This integral can be expressed in terms of the lower incomplete gamma function as

$$P(q, N) = \frac{1}{\nu U^{\frac{1}{2\nu}}} \gamma \left( \frac{1}{2\nu}, U \right) - \frac{1}{\nu U^{\frac{1}{2\nu}}} \gamma \left( \frac{1}{\nu}, U \right) \quad (2)$$

The variable  $U = (qbN^\nu)^2/6$ . To account for polymer-solvent interactions, the random phase approximation (RPA) was combined with  $P(q, N)$  to fit the SANS intensities:

$$I(q) = \Delta\rho^2 \left[ \frac{1}{Nv_p\phi_p P(q, N)} + \frac{1}{v_s(1-\phi_p)} - \frac{2\chi_{ps}}{\sqrt{v_p v_s}} \right]^{-1} + B \quad (3)$$

where  $B$  is the incoherent background,  $\Delta\rho$  is the difference in scattering length density between the polymer (e.g., PNIPAM) and solvent (e.g.,  $D_2O$ ),  $v_p$  is the volume of the monomer ( $\approx 171 \text{ \AA}^3$ ),  $v_s$  is the volume of a solvent molecule ( $30 \text{ \AA}^3$  for  $D_2O$ ,  $97.2 \text{ \AA}^3$  for Ethanol- $d_6$ ),  $\phi_p$  is the polymer volume fraction, and  $\chi_{ps}$  is the interaction parameter between polymer and solvent.

**Spherical Core-Chain Model:** The SANS data of all dodecyl PNIPAM, PnNPAM, PNCAM that self-assemble into micelles were analyzed with a core-chain model, which is a modified version of a form factor originally introduced by Pedersen for block copolymer micelles [12]. The “core” term describes scattering from the core of the micelle and the chain portion comes from the scattering of the polymer chains with an excluded volume parameter  $\nu$ , forming the corona of the micelle. The primary difference between our model and that introduced by Pedersen is the explicit accounting for the excluded volume parameter in the form factor of the polymer chains, which yields information on the conformation of the chains that form the corona. The scattering intensity is given by the sum of four scattering terms.  $F_A(q)$  is the form factor amplitude of the core, which for the polymer micelles, is given by:

$$F_A(q) = \left[ (\rho_{core} - \rho_{solvent}) V_{core} \frac{3j_1(qr_{core})}{qr_{core}} \right] \quad (4)$$

where  $j_1$  is a spherical Bessel function,  $r_{core}$  is the micelle core

radius,  $\rho_i$  is the scattering length density (SLD) of component  $i$ , and  $V_{core}$  is the volume of the core of the micelle. The form factor amplitude for a polymer chain with excluded volume is given by:

$$F_B(q) = \frac{1}{2\nu U^{\frac{1}{2\nu}}} \gamma \left( \frac{1}{2\nu}, U \right) \quad (5)$$

The total scattering intensity is given by the sum of four terms,

$$I(q) = \frac{N_p}{V} \left[ F_A^2(q) + 2\Delta\rho N_c V_c F_A(q) E(q) F_B(q) + \Delta\rho^2 N_c (N_c - 1) V_c^2 F_B(q) E(q)^2 F_B(q) + \Delta\rho^2 N_c V_c^2 P_B(q) \right] S(q) \quad (6)$$

where  $V_c$  is the volume of a single chain, and  $E(q)$  is a propagator function:

$$E(q) = \frac{\sin(qr_{core})}{qr_{core}} \quad (7)$$

For dodecyl PNIPAM<sup>d-f</sup> with  $M_n > 70$  kDa, we approximate the structure factor term as  $S(q) \approx 1$  due to a lower number density of micelles, and, therefore, a negligible correlation between their positions. For dodecyl PNIPAM<sup>a-c</sup>, where a large correlation peak is observed at intermediate values of  $q$ , the Ornstein–Zernike equation is solved with the Percus–Yevick closure to obtain the structure factor  $S(q)$ .

**Dissipative Particle Dynamics (DPD) Simulations.** Coarse-grained DPD simulations were performed using our in-house, parallel DPD software package PD<sup>2</sup> on the Case Western Reserve University High-Performance Computing Cluster and the Oakley Cluster at the Ohio Supercomputer Center. Within DPD, interactions between beads  $i$  and  $j$  are described by a soft repulsive, conservative force,  $\mathbf{F}^{(C)}$ . The random and dissipative forces,  $\mathbf{F}^{(R)}$  and  $\mathbf{F}^{(D)}$ , respectively, serve as a thermostat for the system. The three force terms are expressed as:

$$\mathbf{F}^{(C)} = a_{ij} \omega(r_{ij}) \hat{\mathbf{r}}_{ij} \quad (8)$$

$$\mathbf{F}^{(R)} = \sigma \zeta \omega(r_{ij}) (\Delta t)^{-1/2} \hat{\mathbf{r}}_{ij} \quad (9)$$

$$\mathbf{F}^{(D)} = -\gamma \omega^2(r_{ij}) (\hat{\mathbf{r}}_{ij} \Delta \mathbf{v}_{ij}) \hat{\mathbf{r}}_{ij} \quad (10)$$

where  $a_{ij}$  describes the strength of the interaction, and  $\zeta$  is a uniform random number with zero mean and unit variance.  $\omega(r)$  is a weighting function that decreases linearly from 1 to 0 on the interval  $0 \leq r \leq r_c$ . We take  $r_c = 1$ . The fluctuation-dissipation theorem requires that the coefficients of the random and dissipative forces be related according to:

$$\gamma = \frac{\sigma^2}{2k_B T} \quad (11)$$

In all simulations,  $k_B T = \varepsilon_0 = 1$ , and  $\sigma = 3.00$ . The equations of motions are integrated at each time step using the Velocity-Verlet algorithm, and the simulations were run for at least 500 000 time steps with  $\Delta t = 0.01 \tau$ , at which point the micelle morphology was completely developed. More details on the DPD methodology are available throughout the literature.

To mimic experiments, polymers were modeled as A-B diblock chains containing  $N = 50$  beads, connected together via a harmonic potential, and dispersed in a matrix of solvent beads at a density of  $\rho = 3 r_c^{-3}$ . At  $t = 0$ , the chains were randomly distributed throughout the simulation box, with size  $L_x = L_y = L_z = 64 r_c$ . The polymer

volume fraction of the chains was set to 1% to match experimental conditions. The B block of the chain mimics the hydrophobic ethyl or dodecyl terminal group in the experiments, with a length that was varied from 1 to 29 beads (*i.e.*,  $\phi_B = 0.02$  to 0.58). A-A, B-B, and solvent-solvent (S-S) interactions strengths were set to  $a_{AA} = a_{BB} = a_{SS} = 25\epsilon_0$ , which was shown by Groot and Warren to reproduce the compressibility of water. For simplicity, the A-S and B-S interactions were taken to be  $a_{AS} = 25\epsilon_0$  and  $a_{BS} = 60\epsilon_0$ . The magnitude of the B-S interaction is such that strong segregation occurs between the terminal group and solvent, and the effects of fluctuations are minimized. For each system, five independent runs were performed to eliminate statistical deviations. The aggregation number ( $N_{agg}$ ) was averaged across all five runs.

### 3. Results and discussion

**Thermoresponsive Behavior.** The molecular weights and terminal group chemistries of all polymers are summarized in Table 1. Fig. 3a–c shows SANS measurements of ethyl- and dodecyl-terminated poly(N-alkylacrylamide)s below and close to their critical temperatures. The temperature for each set of measurements is noted in the figure, as it varies based on the particular polymer. For all sets of polymers, scattering from the ethyl-terminated samples (black points) is markedly different from the dodecyl-terminated samples (blue points). The difference is most easily observed in the slopes of the ethyl- and dodecyl-terminated polymers, with the dodecyl-terminated polymers exhibiting steeper slopes at intermediate values of  $q$ , which are indicative of more compact objects, which is in agreement with the literature [16,18,46]. Although the general trends are consistent among the three polymer systems, the differences between ethyl- and dodecyl-terminated polymers are most easily observed in the PNCPAM system (Fig. 3c). The difference between ethyl and dodecyl terminated PNIPAM is smaller than PNPAM and PNCPAM. There are several reasons for this behavior. First, the temperature range of the PNIPAM and PNPAM measurements (15 °C) is smaller than PNCPAM (40 °C) and the measurements are taken close to the critical temperatures in those systems where chains begin to aggregate. Second, the molecular weight of the PNIPAM system shown in Fig. 3 is larger than for the PNPAM and PNCPAM systems, meaning the scattering intensity of the ethyl-terminated polymers is larger and closer to that of the self-assembled dodecyl-terminated chains. Ethyl-terminated polymers exhibit scattering patterns reminiscent of individual polymer chains in solution, whereas for dodecyl-terminated polymers, the increased scattering intensities and presence of a peak at intermediate  $q$  imply scattering from larger particles rather than individual polymer chains. Another notable feature is that at temperatures well below the critical temperature, dodecyl-terminated polymers do not form

**Table 1**  
Poly(N-alkylacrylamide) characteristics from SEC-MALS measurements.

Sample ID	$M_n$ (kg/mol)	$M_w$ (kg/mol)	$\bar{D}$ ( $M_w/M_n$ )	Terminal Group
Ethyl PNIPAM <sup>a</sup>	19.7	20.4	1.04	CH <sub>2</sub> CH <sub>3</sub>
Ethyl PNPAM <sup>b</sup>	86.3	96.7	1.12	CH <sub>2</sub> CH <sub>3</sub>
Ethyl PNPAM	20.3	21.9	1.08	CH <sub>2</sub> CH <sub>3</sub>
Ethyl PNCPAM	21.3	22.8	1.08	CH <sub>2</sub> CH <sub>3</sub>
Dodecyl PNIPAM <sup>a</sup>	19.6	20.4	1.09	(C <sub>2</sub> H <sub>4</sub> ) <sub>5</sub> CH <sub>2</sub> CH <sub>3</sub>
Dodecyl PNIPAM <sup>b</sup>	35.3	38.0	1.08	(C <sub>2</sub> H <sub>4</sub> ) <sub>5</sub> CH <sub>2</sub> CH <sub>3</sub>
Dodecyl PNIPAM <sup>c</sup>	61.5	67.5	1.10	(C <sub>2</sub> H <sub>4</sub> ) <sub>5</sub> CH <sub>2</sub> CH <sub>3</sub>
Dodecyl PNIPAM <sup>d</sup>	76.2	88.1	1.16	(C <sub>2</sub> H <sub>4</sub> ) <sub>5</sub> CH <sub>2</sub> CH <sub>3</sub>
Dodecyl PNIPAM <sup>e</sup>	98.5	121.6	1.24	(C <sub>2</sub> H <sub>4</sub> ) <sub>5</sub> CH <sub>2</sub> CH <sub>3</sub>
Dodecyl PNIPAM <sup>f</sup>	112.5	135.3	1.2	(C <sub>2</sub> H <sub>4</sub> ) <sub>5</sub> CH <sub>2</sub> CH <sub>3</sub>
Dodecyl PNPAM	18.9	20.6	1.09	(C <sub>2</sub> H <sub>4</sub> ) <sub>5</sub> CH <sub>2</sub> CH <sub>3</sub>
Dodecyl PNCPAM	21.9	23.2	1.06	(C <sub>2</sub> H <sub>4</sub> ) <sub>5</sub> CH <sub>2</sub> CH <sub>3</sub>

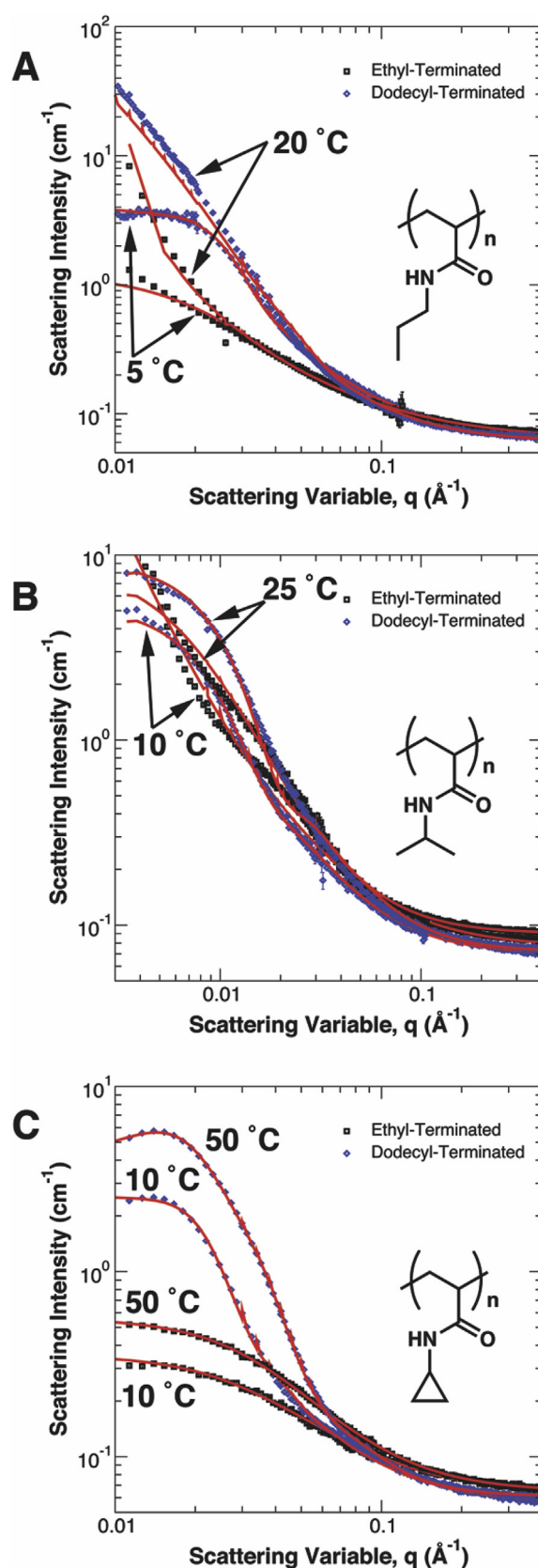


**Fig. 3.** Small-angle neutron scattering (SANS) of (a) ethyl PNPAM, dodecyl PNPAM at 5 °C and 20 °C, (b) ethyl PNIPAM, dodecyl PNIPAM at 10 °C and 25 °C and (c) ethyl PNCPAM, dodecyl PNCPAM at 10 °C and 50 °C. Solid lines are best fits from core-chain model for dodecyl polymers and RPA model for ethyl polymers. Error bars correspond to one standard deviation.

aggregates or clusters, demonstrated by the leveling off of the scattering intensity as  $q$  decreases towards zero. In contrast, the variation in scattering intensity from ethyl-terminated PNnPAM and PNIPAM at low  $q$  can be described by a power law. Power law behavior in the scattering intensity has been observed previously for aqueous poly(ethylene oxide) (PEO) solutions, which Hammouda et al. attributed to association of terminal groups [47]. As temperature increases towards the LCST, several changes are observed. In the PNnPAM system at 20 °C, near its LCST, both the ethyl-terminated polymer and the micelles begin to aggregate as indicated by the power law behavior of the increase in scattering intensities for both samples at low  $q$ . For PNIPAM and PNCPAM, both of which are below their LCSTs of 32 °C and 60 °C, respectively, the scattering intensity increases with temperature, confirming the LCST behavior seen previously by others. Ethyl-terminated PNIPAM begins to cluster, as has been observed previously [7], but the PNIPAM micelles remain dispersed at 25 °C. In contrast to both PNnPAM and PNIPAM, the SANS does not show any indication of clustering of PNCPAM with either terminal group, and the PNCPAM micelles remain dispersed at up to 50 °C, perhaps due to the increased hydrophilicity and reduced surface area of the cyclopropyl group relative to the other polymers. To further investigate the behavior of the polymers with respect to temperature, SANS measurements were taken at several temperatures below the LCST of each polymer. Fig. 4 plots the scattering intensity for ethyl terminated PNCPAM in D<sub>2</sub>O as a function of temperature. The complete set of SANS measurements and fits of all ethyl polymers are contained in the Supporting Information (Figs. S9–S10). Analysis using the RPA allowed us to extract conformation and interaction parameters between each polymer and D<sub>2</sub>O as a function of temperature, which are described in more detail below. The PNCPAM data confirms that the polymer does not cluster in solution, as was observed for PNnPAM and PNIPAM. Interestingly, this observation may imply that the clustering previously observed in PNIPAM solutions below the LCST may not be solely due to terminal group effects, but perhaps the relative hydrophilicity of the monomer relative to the terminal groups. From the values of the

interaction parameter extracted by the RPA analysis, PNnPAM is the most hydrophobic polymer of the three analogs, and PNCPAM is the least hydrophobic. The complete set of interaction parameter of ethyl polymers are contained in the Supporting Information (Fig. S11).

Ito and Kubota found evidence of association of the n-propyl chains on the n-propyl acrylamide monomer in aqueous PNnPAM solutions (0.1 wt%) below the theta temperature, and it has been suggested that PNIPAM exhibits  $n$ -clustering behavior, which is characterized an effective attraction between chains despite favorable interactions between the monomers and solvent [19–21]. Ito and Kubota attributed the association of the n-propyl chains to intramolecular interactions within the PNnPAM chains. At higher concentrations of polymer, such as in the micelles formed by the dodecyl-terminated polymers, it is likely that intermolecular interactions would become an increasingly important aspect of the clustering/association behavior of the poly(N-alkylacrylamide)s. Although the idea that intermolecular associations lead to clustering of PNIPAM and PNnPAM might seem at odds with the fact that poly(N-alkylacrylamide) micelles are stable in solution, SANS measurements indicate changes in the micellar structure that would be consistent with intermolecular association within the particles. Fits to the SANS intensities using the core-chain mode in Eq. (6) can directly extract the excluded volume parameter  $\nu$  (i.e., Flory exponent), where the mean radius of gyration of the chains in the corona scales with the degree of polymerization  $N$  as  $R_g \sim N^\nu$ . Ethyl-terminated polymers can be analyzed with the excluded volume model in Eq. (3). An ideal chain has  $\nu = 0.5$ , whereas a polymer in a good solvent has  $\nu \approx 0.6$ . When a chain collapses into a globule,  $\nu \approx 0.3$ . Previous studies using the model in Eq. (5) have successfully reproduced expected values of  $\nu$ , establishing the validity of the core-chain model to determining chain conformation [7,48–50]. Fig. 5 plots the excluded volume parameter of all polymer systems as a function of temperature, with ethyl-terminated polymers shown as dashed lines, and dodecyl-terminated polymers shown as solid lines. The complete set of SANS fits of dodecyl polymers are contained in the Supporting Information (Figs. S12–S14). The lines

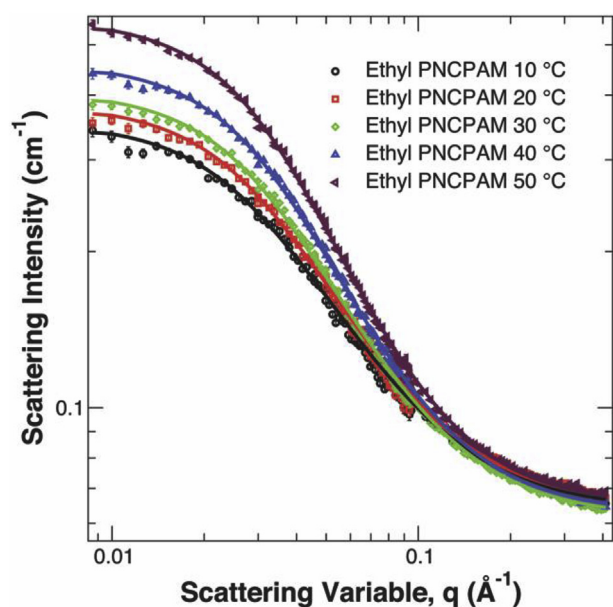


**Fig. 4.** Small-angle neutron scattering (SANS) for ethyl PNCPAM at 10 °C (Black), 20 °C (red), 30 °C (green), 40 °C (blue), and 50 °C (magenta) in D<sub>2</sub>O. The solid lines are best fits according to eq (3). The error bars correspond to one standard deviation. (For interpretation of the references to color in this figure legend, the reader is referred to the Web version of this article.)

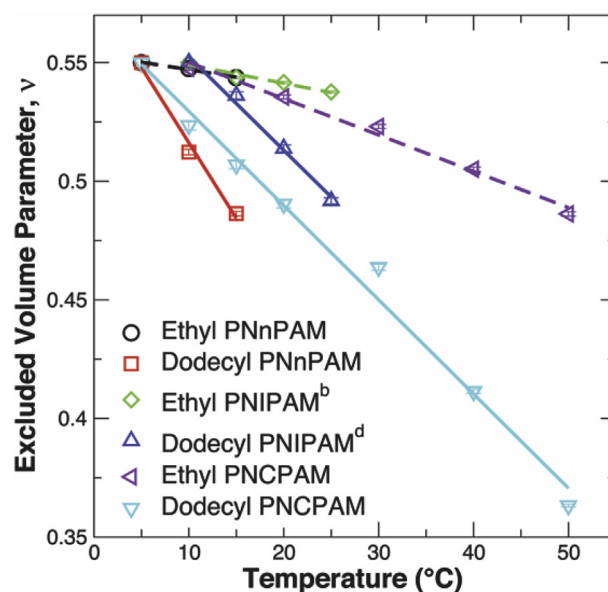


**Fig. 5.** Excluded volume parameter ( $\nu$ ) extracted from least squares fitting of the SANS data to the RPA model in eq (3) for ethyl polymers and core chain model for dodecyl polymers in Eq. (6), respectively. Dashed lines correspond to ethyl polymers and solid lines to dodecyl polymers. Lines are guides to the eye. Error bars are smaller than the data points, and correspond to one standard deviation.

from ethyl-terminated polymers follow the same general trend, with  $\nu$  decreasing monotonically from 0.55 to slightly below 0.50 for PNCPAM at  $T = 50^\circ\text{C}$ . Because of strong clustering of PNnPAM and PNIPAM, determining the conformation at temperatures greater than  $15^\circ\text{C}$  and  $20^\circ\text{C}$ , respectively, is difficult due to the combination of scattering from individual polymer chains and from the clusters of chains. In contrast to ethyl-terminated polymers, the dodecyl-terminated polymers display a greater decrease in the excluded volume parameter with respect to temperature. For PNCPAM, which has the largest accessible temperature window for determining chain conformation,  $\nu$  decreases from 0.55 to almost 0.35 as  $T$  increases from  $10^\circ\text{C}$  to  $50^\circ\text{C}$ , near the LCST. We observe that all dodecyl polymers (solid lines) experience a stronger temperature dependence than the ethyl polymers (dashed lines). The dodecyl polymers exhibit a more compact conformation, which is consistent with our star-branched PNIPAM study [23]. In the case of star-branched PNIPAM, we concluded that the polymers must be aggregating with one another and forming compact globules based on the fact that the size of the polymers increased slightly to approximately twice the  $R_g$  of an individual polymer chain in solution, and that the excluded volume parameter remained constant near  $\nu \approx 0.38$  for the temperature range of  $5^\circ\text{C}$  to  $20^\circ\text{C}$ . For the dodecyl-terminated polymers in the present study, we reason that the behavior is distinct from the case of star-branched polymers. In the polymer micelles, the concentration of monomers increases as the distance to the core of the micelle decreases. Shan et al. performed microcalorimetry measurements on spherical Au nanoparticles that were grafted with  $\alpha$ -thiol  $\omega$ -carboxyl terminated PNIPAM, and found two distinct phase transitions of the polymer [29]. Portions of the chain near the Au core collapsed at temperatures below the typical LCST due to an increase in monomer concentration, while portions of the chain farther away from the nanoparticle core collapsed over a wider temperature range closer to the LCST. A continuous collapse of PS-*b*-PNIPAM micelles has been observed by Zhang et al. [51], and Luo et al. [52] observed a double phase transition in PNIPAM dendrimers with a hydrophobic core, indicating that this behavior extends to micellar and certain unimolecular systems as well. Our micelles exhibit a similar monomer concentration gradient as a function of distance from the micelle core but have much smaller core sizes (*i.e.*, higher curvature) than micelles formed from block copolymers, and much lower local concentrations of polymer than in the studies of Shan et al. and Luo et al. Nevertheless, we hypothesize that the lower excluded volume parameters we observe, relative to the free ethyl-terminated polymers, arise from the increased polymer density in the micelles which lead to collapse of the chains below the LCST. At the same time, the micelles remain soluble due to the portions of the chain that are farther away from the micelle core. The values extracted from the spherical core-chain model represent an average conformation across the contour of the polymer chain. Taken together, these results suggest *n*-clustering behavior in all three of the dodecyl-terminated poly(N-alkylacrylamides) we studied, and that this is distinct from the clustering/association that is observed for the ethyl-terminated polymers.

The distinct assemblies of the ethyl- and dodecyl-terminated polymers suggest that their thermoresponsive behaviors may be different, and turbidimetry measurements of the six polymer systems confirm that this is the case. Heating curves for ethyl- (black) and dodecyl-terminated (red) poly(N-alkylacrylamide)s at a concentration of 0.5 wt% are shown in Fig. 6. In the case of PNnPAM and PNCPAM, the dodecyl-terminated polymers show a lower cloud point temperature than the ethyl-terminated polymers, presumably due to the more hydrophobic dodecyl groups. Interestingly, PNIPAM does not display this trend in the position of the cloud point temperatures, and the cloud point of dodecyl-terminated

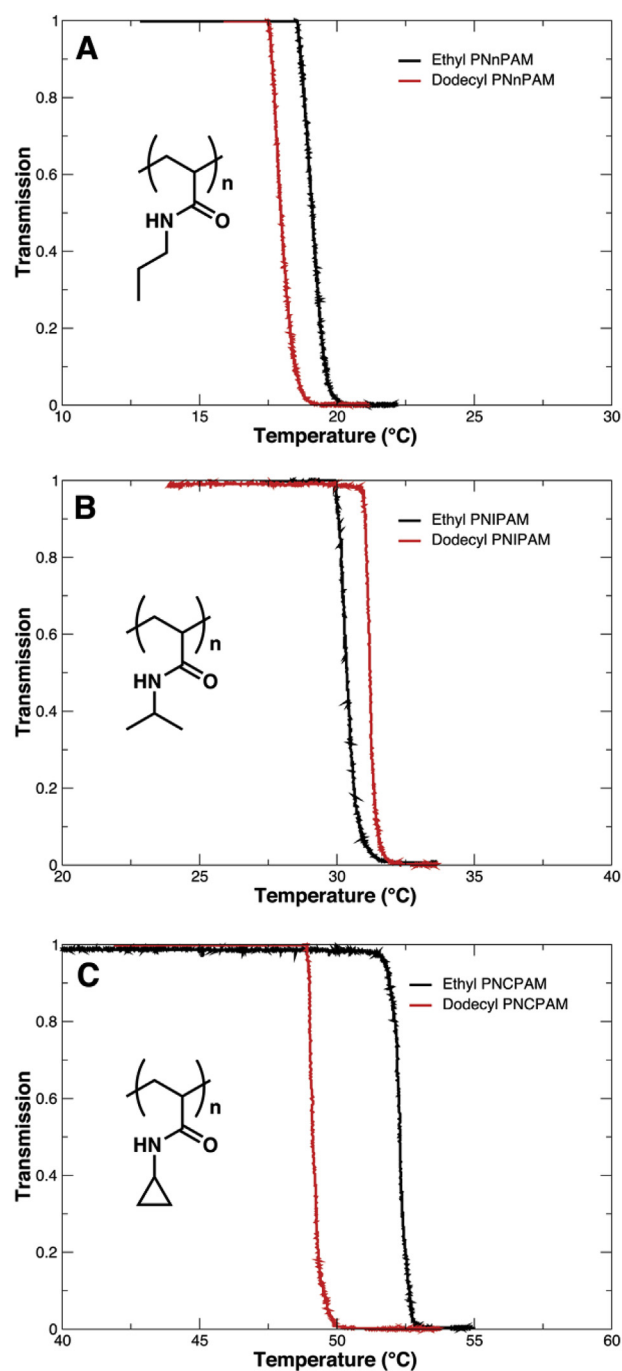


**Fig. 6.** Turbidimetry measurements of (a) PNnPAM (b) PNIPAM and (c) PNCPAM in water as a function of temperature. Black lines correspond to ethyl-terminated polymers, and red lines correspond to dodecyl-terminated polymers. (For interpretation of the references to color in this figure legend, the reader is referred to the Web version of this article.)

PNIPAM is higher than that of ethyl-terminated PNCPAM.

Chung et al. [30], previously found that the cloud point temperature of PNIPAM with long alkyl chains is dependent upon whether the solution is above or below the critical micelle concentration (CMC), implying that the polymer assembly plays a role in the thermoresponsive behavior. While our dodecyl-terminated polymers form micelles below the LCST, the SANS measurements of PNIPAM (Fig. 3b) do not indicate as large of a difference between the scattering patterns of the dodecyl- and ethyl-terminated

polymers (Fig. 3a–c, respectively). We do not have a satisfactory explanation of the different behavior of the PNIPAM system at the moment relative to PNNPAM and PNCPAM, except to note that there may be structural differences which should be investigated further in future studies.

**Micellization and Micelle Structure.** To probe the structure of the assemblies of dodecyl-terminated PNIPAM, we synthesized a series of low dispersity polymers with varying molecular weight. SANS measurements (data points) of dodecyl PNIPAM with different  $M_n$  at 10 °C, fit with the core–chain model (solid lines), are shown in Fig. 7. The polymer molecular weight increases from a to f. The radius of the micelle core was found to be approximately  $r_{core} \approx 6$  nm for PNIPAM<sup>a</sup>, and increased with the molecular weight of the polymer to a maximum of  $r_{core} \approx 12$  nm for PNIPAM<sup>f</sup>. The radius of the micelle core was constant with respect to temperature, indicating that it must be formed from the dodecyl groups, as well as a portion of collapsed polymer. The core radius was similar for low molecular weight PNNPAM and PNCPAM micelles. Scattering from low molecular weight polymers – dodecyl PNIPAM<sup>a</sup> and PNIPAM<sup>b</sup> – shows a strong peak near  $q = 0.015 \text{ \AA}^{-1}$  due to interparticle scattering (i.e., the peak is from the structure factor,  $S(q)$ ). In addition, we observe that the magnitude of the structure factor decreases with increasing  $M_n$  to the point that at higher molecular weights, the structure factor  $S(q) \approx 1$ . This observation is attributed to the fact that at fixed mass fractions, the number density of polymer chains decreases as  $M_n$  increases, leading to a smaller number of micelles in solution; thus, the intermicellar distance is expected to increase resulting in both a shift of the structure factor peaks to lower  $q$  as well as a reduction in the magnitude of the associated peaks.

Although we cannot obtain an interaction parameter by fitting SANS data with the core–chain model, we can further understand the micelle structure through both the excluded volume parameter as well as an estimate of the aggregation number  $N_{agg}$ . Fig. 8 shows  $N_{agg}$  as a function of temperature of dodecyl PNIPAM with different  $M_n$ .  $N_{agg}$  decreases slightly with increasing  $M_n$  from approximately 15 for PNIPAM<sup>a</sup> to 4 for PNIPAM<sup>f</sup>, which we hypothesize is likely due to increased shielding of the micelle core as the polymer chains

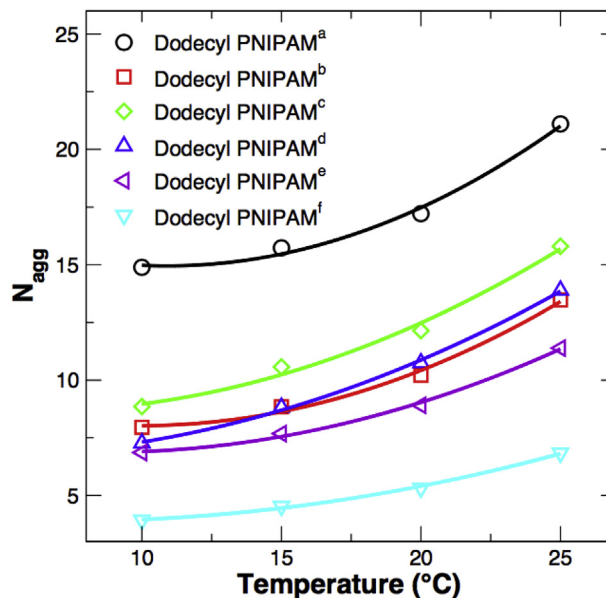


Fig. 8.  $N_{agg}$  as a function of temperature for dodecyl PNIPAM<sup>a–f</sup>.

become longer, preventing additional chains from joining the assembly. The values of  $N_{agg}$  for PNIPAM<sup>b–d</sup> are within a narrow range (e.g. 7 to 8.8 at 10 °C) and  $N_{agg}$  of PNIPAM<sup>b</sup> is slightly lower than PNIPAM<sup>c</sup>. Considering the error bars of  $N_{agg}$ ,  $N_{agg}$  is not very sensitive variations in  $M_n$  and  $N_{agg}$  for PNIPAM<sup>b–d</sup> are similar to each other without significant differences ( $M_n$  of 35 kg/mol to 98 kg/mol). This observation is also in agreement with previous work from the O'Reilly and Epps groups [46].  $N_{agg}$  for all dodecyl PNIPAM increases slightly with increasing temperature, confirming that the polymer–polymer interaction is becoming stronger. Because the increase in  $N_{agg}$  is subtle, this may be attributed free chains in solution joining the micelles as interactions between the polymer and solvent become increasingly unfavorable. Fig. 9 plots the excluded

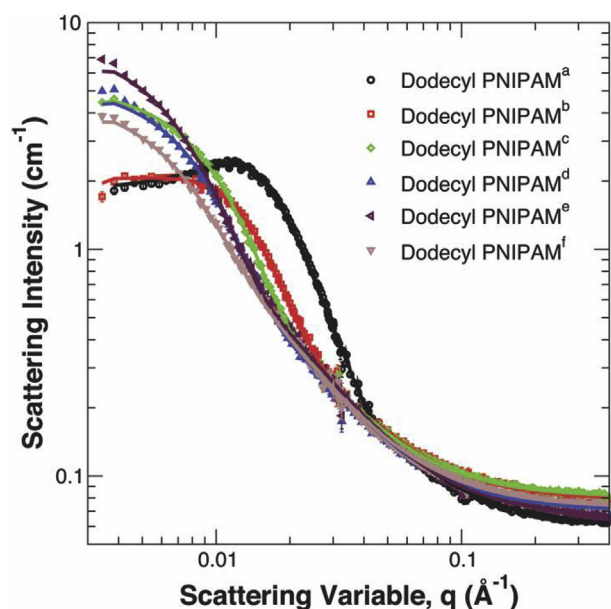


Fig. 7. Small-angle neutron scattering (SANS) for dodecyl PNIPAM (a–f) at 10 °C. Error bars correspond to one standard deviation, and are smaller than the data points. Lines are best fits from core–chain model.

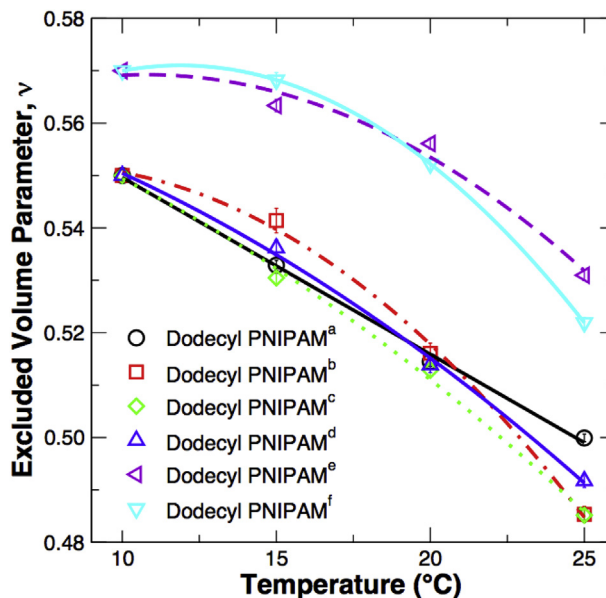
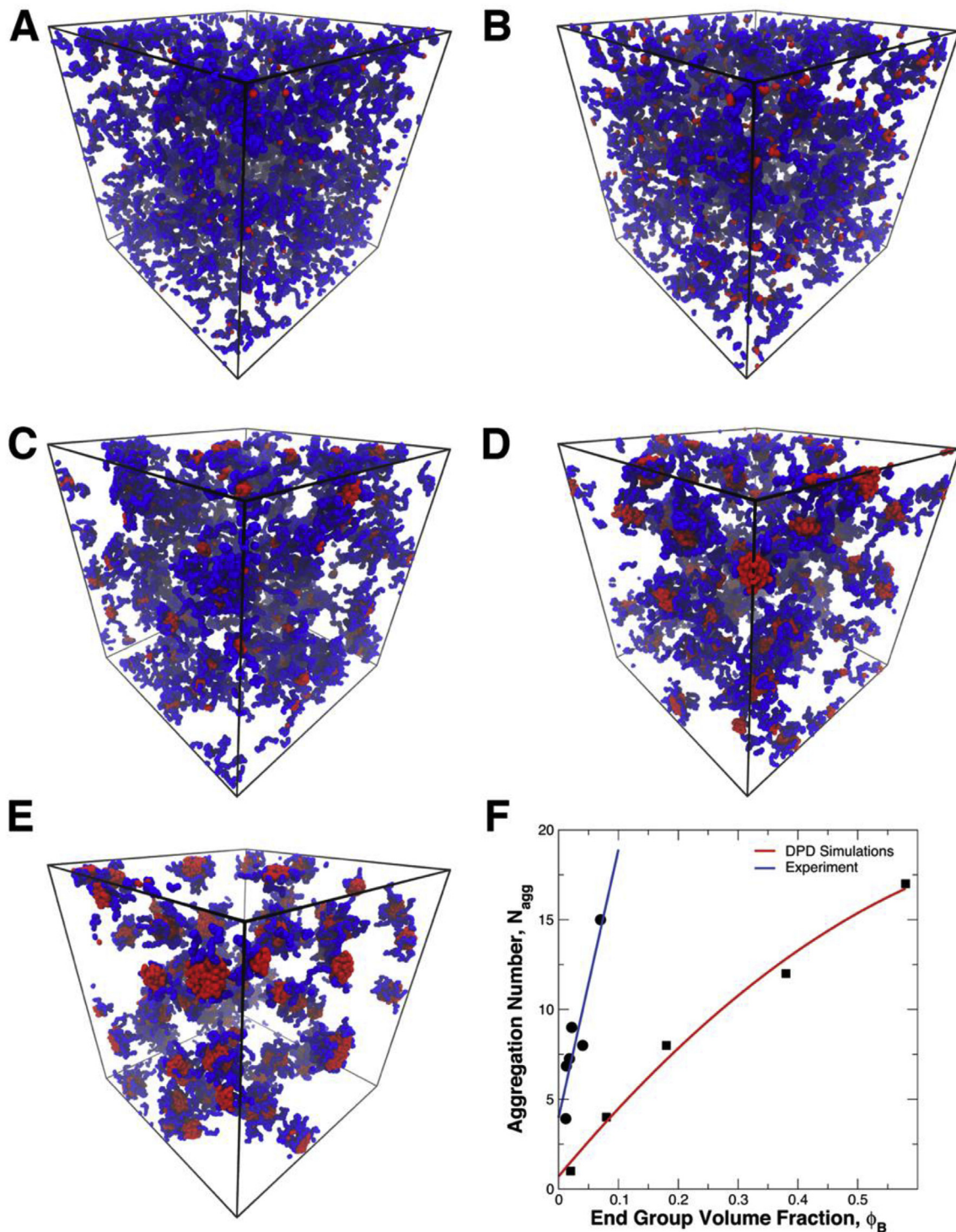


Fig. 9. Excluded volume parameter ( $v$ ) of dodecyl PNIPAM<sup>a–f</sup> in  $D_2O$  at 10 °C, 15 °C, 20 °C and 25 °C. Least squares fitting was used to fit the SANS data to the core–chain model in Eq. (6). Solid and dashed lines are guides to the eye. Error bars are smaller than the data points, and correspond to one standard deviation.

volume parameter as a function of temperature for dodecyl PNIPAM with different  $M_n$ . The decrease of  $v$  with increasing temperature corresponds to LCST behavior and  $M_n$  has no significant effect on this behavior, as indicated by the similar values of  $v$  and the similar slopes of the trends with respect to temperature. As discussed in the previous section, the steepness of the slopes, relative to the ethyl-terminated polymers, indicates that the polymers are

collapsing at lower temperatures and more dramatically when in a micellar structure. This behavior is attributed to  $n$ -clustering of PNIPAM due to the higher local concentration of polymer when it assembles.

For the highest molecular weight polymers, PNIPAM<sup>e</sup> and PNI-PAM<sup>f</sup>, the values of  $v$  that we obtain are higher than for the other polymers in the series. This may be due to two effects. First, the



**Fig. 10.** Snapshots of system morphology from DPD simulations as a function of increasing terminal group volume fraction (i.e., decreasing chain length). (a–e) correspond to terminal group volume fractions of  $\phi_B = 0.02, 0.08, 0.18, 0.38,$  and  $0.58$ , respectively. (f) Average aggregation number ( $N_{agg}$ ) for the systems in (a–e) (squares), averaged across five independent runs, along with  $N_{agg}$  for the experimental system at  $T = 10^\circ\text{C}$  (circles). Lines are guides to the eye. For clarity, solvent particles are not shown.

dispersity of these polymers ( $\mathcal{D} > 1.2$ ) is considerably higher than the other polymers in the series, and fits to the SANS data may not be as reliable in this case. Secondly, the higher molecular weights of these polymers may be such that a larger portion of the chain is in the dilute region where  $n$ -clustering does not occur, leading to a larger effective excluded volume parameter.

DPD simulations were performed to qualitatively predict whether the structures inferred from neutron scattering measurements were likely to form. Quantitative comparisons between simulations and experiments are not possible due to differences between the simple, soft repulsive interactions in DPD and the more complex interactions in the experimental system, which can include attractive interactions such as hydrogen bonding; thus, the DPD simulations primarily explore the effect of terminal group hydrophobicity on the assembly of the polymer chains. In addition, exact comparisons between DPD simulations and experiments are further complicated by the fact that mapping the DPD temperature to the experimental temperature is difficult. Fig. 10a–e shows snapshots of the configurations of the systems after 500,000 time steps as the volume fraction of the terminal group ( $\phi_B$ ), relative to the hydrophilic portion of the chain, increases. The hydrophobic core is shown in red, and the hydrophilic corona is shown in blue. Solvent particles are not shown. At the lowest value of  $\phi_B = 0.02$  (Fig. 10a), no micelles form ( $N_{agg} = 1$ ). Fig. 10 plots the aggregation number as a function  $\phi_B$  (squares), along with  $N_{agg}$  for the data in Fig. 8 at 10 °C (circles). Because the volume of the dodecyl group relative to the NIPAM monomer is unknown, the x-axis values represent the number fraction of the terminal group versus the polymer chain for the experimental system. Although the numbers are not in quantitative agreement, we observe that the values of  $N_{agg}$  determined experimentally are reasonably close to those predicted by DPD, and that they decrease as the length of the chain, relative to the terminal group, increases. The DPD results support the interpretation of the neutron scattering measurements.

#### 4. Summary

In summary, we have examined the thermoresponsive behavior of three closely related poly(N-alkylacrylamide)s as a function of molecular weight and terminal group. SANS measurements allowed us to separately examine both the structure of the core and corona of micelles formed from dodecyl-terminated polymers, and to extract thermodynamic information from the ethyl-terminated polymers that exist as individual polymer chains in solution. By analyzing the SANS measurements we observed that the increased hydrophobicity of dodecyl terminal group (compared to the ethyl group) promotes polymer chain self-assembly into micelles. SANS measurements found that dodecyl-terminated poly(N-alkylacrylamide)s exhibit a more compact conformation than the ethyl terminated polymers at a given temperature, and that dodecyl-terminated polymers do not form aggregates or clusters below the critical temperature in the same manner as ethyl-terminated polymers. Except for PNCPAM, ethyl-terminated polymers begin to cluster at temperature below the LCST, as previous observed, implying that PNIPAM clustering below the LCST comes not only from terminal group effects, but may also depend on the relative hydrophilicity of the monomer relative to the terminal groups. The clustering observed from SANS measurements does not appear in turbidimetry measurements, and the solutions appear colorless. In contrast, dodecyl-terminated polymers remain dispersed as individual particles at temperatures up to the LCST. Excluded volume parameters extracted from SANS reveal that dodecyl-terminated polymers experience a stronger temperature dependence and are more compact than the ethyl-terminated polymers. The origin of this behavior is strong polymer-polymer interactions arising from

an increased polymer density close to the core of micelles (“ $n$ -clustering”), which has been previously observed in some polymer systems. The results of this study are especially relevant in designing responsive polymeric micelles, and in understanding the contributions that monomer and terminal group characteristics impart to thermoresponsive materials that are composed of similar polymers.

#### Acknowledgements

Access to the NGB 30 m SANS instrument was provided by the Center for High Resolution Neutron Scattering (CHRNS), a partnership between the National Institute of Standards and Technology and the National Science Foundation under Agreement No. DMR-1508249. The identification of commercial products or experimental methods does not imply endorsement by NIST, nor does it imply that these are the best for the purpose. MJAH and XL acknowledge partial support of this research by a National Science Foundation CAREER Award from the Polymers program (DMR-1651002). This work made use of the Oakley Supercomputer at the Ohio Supercomputer Center, as well as the High Performance Computing Resource in the Core Facility for Advanced Research Computing at Case Western Reserve University. The authors thank Erin Xu (Hathaway Brown) for assistance in turbidimetry measurements and Xiaozhou Shen (University at Buffalo) for help with micelle figure design.

#### Appendix A. Supplementary data

Supplementary data related to this article can be found at <https://doi.org/10.1016/j.polymer.2018.04.068>.

#### References

- [1] X.L. Sun, P.C. Tsai, R. Bhat, E.M. Bonder, B. Michniak-Kohn, A. Pietrangelo, *J. Mater. Chem. B* 3 (5) (2015) 814–823.
- [2] Y. Guan, Y. Zhang, *Soft Matter* 7 (14) (2011) 6375–6384.
- [3] T. Kawano, Y. Niidome, T. Mori, Y. Katayama, T. Niidome, *Bioconjugate Chemistry* 20 (2) (2009) 209–212.
- [4] M. Heskins, J.E. Guillet, *J. Macromol. Sci.-Chem.* 2 (8) (1968) 1441–1455.
- [5] C. Wu, S. Zhou, *Phys. Rev. Lett.* 77 (14) (1996) 3053.
- [6] C. Wu, X. Wang, *Phys. Rev. Lett.* 80 (18) (1998) 4092.
- [7] M.J. Hore, B. Hammouda, Y. Li, H. Cheng, *Macromolecules* 46 (19) (2013) 7894–7901.
- [8] R.O. Costa, R.F. Freitas, *Polymer* 43 (22) (2002) 5879–5885.
- [9] J.F. Douglas, J. Dudowicz, F. Karl, *J. Chem. Phys.* 143 (2015) 131101.
- [10] I. Bischofberger, D.C.E. Calzolari, P. De Los Rios, I. Jelezarov, V. Trappe, *Sci. Rep.* 4 (2014) 4377.
- [11] S. Furyk, Y. Zhang, D. Ortiz-Acosta, P.S. Cremer, D.E. Bergbreiter, *J. Polym. Sci. Polym. Chem.* 44 (4) (2006) 1492–1501.
- [12] H. Yim, M. Kent, S. Mendez, G. Lopez, S. Satija, Y. Seo, *Macromolecules* 39 (9) (2006) 3420–3426.
- [13] Z. Tong, F. Zeng, X. Zheng, T. Sato, *Macromolecules* 32 (13) (1999) 4488–4490.
- [14] Y. Xia, N.A.D. Burke, H.D.H. Stover, *Macromolecules* 39 (6) (2006) 2275–2283.
- [15] A. Halperin, M. Kröger, F.M. Winnik, *Angew. Chem. Int. Ed.* 54 (51) (2015) 15342–15367.
- [16] P.A. FitzGerald, S. Gupta, K. Wood, S. b Perrier, G.G. Warr, *Langmuir* 30 (27) (2014) 7986–7992.
- [17] J. Skvarla, R.K. Raya, M. Uchman, J. Zedník, K. Procházka, V.M. Garamus, A. Meristoudi, S. Pispas, M. Štěpánek, *Colloid Polym. Sci.* 295 (8) (2017) 1343–1349.
- [18] T. Koga, F. Tanaka, R. Motokawa, S. Koizumi, F.M. Winnik, *Macromolecules* 41 (23) (2008) 9413–9422.
- [19] D. Ito, K. Kubota, *Macromolecules* 30 (25) (1997) 7828–7834.
- [20] H. Inomata, S. Goto, S. Saito, *Macromolecules* 23 (22) (1990) 4887–4888.
- [21] D. Ito, K. Kubota, *Polymer Journal* 31 (3) (1999) 254–257.
- [22] G. Moad, Y. Chong, A. Postma, E. Rizzardo, S.H. Thang, *Polymer* 46 (19) (2005) 8458–8468.
- [23] X. Lang, W.R. Lenart, J.E. Sun, B. Hammouda, M.J. Hore, *Macromolecules* 50 (5) (2017) 2145–2154.
- [24] Y. Li, B.S. Lokitz, C.L. McCormick, *Macromolecules* 39 (1) (2006) 81–89.
- [25] A. Li, H.P. Luehmann, G. Sun, S. Samarajeewa, J. Zou, S. Zhang, F. Zhang, M.J. Welch, Y. Liu, K.L. Wooley, *ACS Nano* 6 (10) (2012) 8970–8982.
- [26] A.W. York, S.E. Kirkland, C.L. McCormick, *Adv. Drug Deliv. Rev.* 60 (9) (2008)

- 1018–1036.
- [27] E.G. Kelley, J.N. Albert, M.O. Sullivan, T.H. Epps III, *Chem. Soc. Rev.* 42 (17) (2013) 7057–7071.
- [28] H. Huang, E.E. Remsen, T. Kowalewski, K.L. Wooley, *J. Am. Chem. Soc.* 121 (15) (1999) 3805–3806.
- [29] J. Shan, J. Chen, M. Nuopponen, H. Tenhu, *Langmuir* 20 (11) (2004) 4671–4676.
- [30] J. Chung, M. Yokoyama, K. Suzuki, T. Aoyagi, Y. Sakurai, T. Okano, *Colloids Surfaces B Biointerfaces* 9 (1–2) (1997) 37–48.
- [31] M.T. Savoji, S. Strandman, X. Zhu, *Macromolecules* 45 (4) (2012) 2001–2006.
- [32] D. Xie, X. Ye, Y. Ding, G. Zhang, N. Zhao, K. Wu, Y. Cao, X. Zhu, *Macromolecules* 42 (7) (2009) 2715–2720.
- [33] C. Zhou, M.A. Hillmyer, T.P. Lodge, *Macromolecules* 44 (6) (2011) 1635–1641.
- [34] P.W. Zhu, D.H. Napper, *Macromolecules* 32 (6) (1999) 2068–2070.
- [35] H. Chen, J. Li, Y. Ding, G. Zhang, Q. Zhang, C. Wu, *Macromolecules* 38 (10) (2005) 4403–4408.
- [36] A. Papagiannopoulos, J. Zhao, G. Zhang, S. Pispas, A. Radulescu, *Polymer* 54 (23) (2013) 6373–6380.
- [37] W. Zhang, L. Shi, K. Wu, Y. An, *Macromolecules* 38 (13) (2005) 5743–5747.
- [38] S. Cammas, K. Suzuki, C. Sone, Y. Sakurai, K. Kataoka, T. Okano, *J. Contr. Release* 48 (2) (1997) 157–164.
- [39] J. Yin, Y. Chen, Z.-H. Zhang, X. Han, *Polymers* 8 (7) (2016) 268.
- [40] P. Kujawa, F. Segui, S. Shaban, C. Diab, Y. Okada, F. Tanaka, F.M. Winnik, *Macromolecules* 39 (1) (2006) 341–348.
- [41] W. Wang, C. Gao, Y. Qu, Z. Song, W. Zhang, *Macromolecules* 49 (7) (2016) 2772–2781.
- [42] P.-G. de Gennes, *Simple Views on Condensed Matter*, 4, 1992, p. 217.
- [43] E. Sevick, *Macromolecules* 31 (10) (1998) 3361–3367.
- [44] A. Halperin, *Eur. Phys. J. B Condens. Matter and Complex Systems* 3 (3) (1998) 359–364.
- [45] B. Hammouda, *J. Res. Natl. Inst Stan* 121 (2016) 139–164.
- [46] J.P. Patterson, E.G. Kelley, R.P. Murphy, A.O. Moughton, M.P. Robin, A. Lu, O. Colombani, C. Chassenieux, D. Cheung, M.O. Sullivan, *Macromolecules* 46 (15) (2013) 6319–6325.
- [47] B. Hammouda, D.L. Ho, S. Kline, *Macromolecules* 37 (18) (2004) 6932–6937.
- [48] M.J. Hore, J. Ford, K. Ohno, R.J. Composto, B. Hammouda, *Macromolecules* 46 (23) (2013) 9341–9348.
- [49] A.V. Zhukhovitskiy, J. Zhao, M. Zhong, E.G. Keeler, E.A. Alt, P. Teichen, R.G. Griffin, M.J. Hore, A.P. Willard, J.A. Johnson, *Macromolecules* 49 (18) (2016) 6896–6902.
- [50] A.V. Zhukhovitskiy, M. Zhong, E.G. Keeler, V.K. Michaelis, J.E. Sun, M.J. Hore, D.J. Pochan, R.G. Griffin, A.P. Willard, J.A. Johnson, *Nat. Chem.* 8 (1) (2016) 33–41.
- [51] W. Zhang, X. Zhou, H. Li, Y. Fang, G. Zhang, *Macromolecules* 38 (3) (2005) 909–914.
- [52] S. Luo, J. Xu, Z. Zhu, C. Wu, S. Liu, *J. Phys. Chem. B* 110 (18) (2006) 9132–9139.